



Received on 08 January 2021; received in revised form, 19 May 2021; accepted, 20 May 2021; published 01 June 2021

DECIPHERING COVID-19 ENIGMA BY TARGETING SARS-COV-2 MAIN PROTEASE USING *IN-SILICO* APPROACHES

M. E. Sobhia^{*}, K. Ghosh, S. Sivangula and G. S. Kumar

Department of Pharmacoinformatics, National Institute of Pharmaceutical Education and Research (NIPER), Mohali - 160062, Punjab, India.

Keywords:

Repurposing, Molecular docking,
Molecular dynamics, SARS-CoV-2,
Main protease

Correspondence to Author:

M. E. Sobhia

Department of Pharmacoinformatics,
National Institute of Pharmaceutical
Education and Research (NIPER),
Mohali - 160062, Punjab, India.

E-mail: mesophia@niper.ac.in

ABSTRACT: Covid-19 pandemic has enforced the entire scientific community to work together and find a solution for the adversity the whole world is facing. This has called for immediate actions, and the most common point of discussion and rapid way to tackle this is to repurpose the previously approved molecules and check their activity against this virus. The role of computational techniques has paved the way for rapid screening of molecules so as to provide us an insight on to designing drugs to inhibit this virus. Our group has screened the Dug bank database containing 8696 molecules. These molecules were screened using three tired molecular docking protocol. We utilized 5R82 as our target structure for the main protease enzyme of SARS-CoV-2, as it was the best available structure in Protein Data Bank. After screening the database, we obtained 200 molecules having docking scores better than the standard molecules (Ritonavir and Lopinavir). Eventually, after detailed analysis, we selected three molecules DB02307, DB04226, and DB01713, for Molecular dynamics simulation study and also compared them with standard molecules. The results clearly show these molecules can potentially act as the main protease inhibitor either by further optimization or repurposing the drug. The wait for the drug continues, but the repurposing strategy surely reveals the ray of hope.

INTRODUCTION: The current outbreak of the novel coronavirus first reported on 31st December 2019 with the cluster reports of positive cases widely spread from the Hubei province of China to many other countries. And it's been over one year, but still, we are in search of the remedy. As of now, 3,418,989 people have lost their lives, and 164,909,216 cases have been reported all around the world (<https://www.worldometers.info/coronavirus/>).

To flatten the curve of the COVID-19 cases, many countries around the world had imposed lockdown. But due to the fear of economic collapse, many countries like the USA, Italy, Russia, India, etc., have imposed relaxation on lockdown. This has eventually increased the risk of infection spread among the people, provided they follow strict rules of "Social distancing" and avoid unwanted social gatherings.

Since there is a fear of possible growth in the second wave, some European countries have planned to impose lockdown again. Hence we all are totally dependent on the arrival of vaccines for COVID-19 as of now. Research groups have been working on developing the vaccines as well as looking forward to approaches like convalescent plasma transfusion¹ and drug repurposing.

QUICK RESPONSE CODE 	DOI: 10.13040/IJPSR.0975-8232.12(6).3104-19
	This article can be accessed online on www.ijpsr.com
DOI link: http://dx.doi.org/10.13040/IJPSR.0975-8232.12(6).3104-19	

Drug repositioning or drug repurposing is the identification of new therapeutic uses for the approved drugs^{2,3}. In the past, numerous successes have been achieved *via* this approach that includes Sildenafil (Viagra), Thalidomide, Clotrimazole, *etc.*⁴ This is an attractive approach because of minimal clinical trial steps required for the medicine to reach the market; also it requires very less investment of time and money. Additionally, this could facilitate the discovery of new mechanisms of action for old drugs⁵ and rapidly advance projects into disease-specific treatments⁶.

The COVID-19 pandemic has called upon immediate use of this approach and is currently being sought to develop safe and effective COVID-19 treatments^{3,7}. Many approved drugs having antiparasitic, antiviral activities have been identified as potential COVID-19 treatments, as shown in **Fig. 1**. As per Excelra COVID-19 Drug Repurposing Database, till now, 128 approved drugs are identified as potential candidates, and many of them are under trial investigations (<https://www.excelra.com/covid-19-drug-repurposing-database/>).

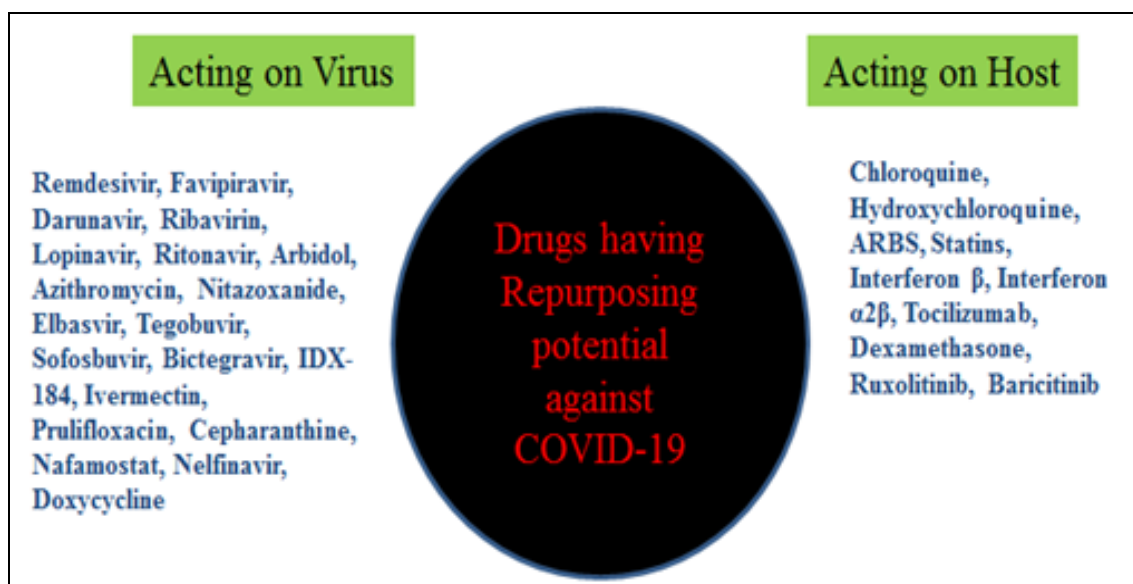


FIG. 1: LIST OF DRUGS HAVING POTENTIAL ACTIVITY AGAINST SARS-COV-2

The disease state of COVID-19 can be classified into three different host inflammatory response phases, namely, (a) Stage I (Early Infection) (b) Stage II (Pulmonary Phase), and (c) Stage III (Hyper inflammation Phase)⁸. The covid-19 virus is a single-stranded positive-sense RNA, that belongs to beta coronavirus family and due to its crown shape called as Coronavirus. This virion is made up of structural proteins namely Envelope (E), Spike (S), Membrane (M), and non-structural proteins (NSP1 to NSP16)^{9,10}.

Key Target Proteins: To select and study key targets is a vital step in identifying drugs with high target specificity or unravelling existing drugs that could be repurposed to treat SARS-CoV-2 infection. **Table 1** list the potential targets that may have a role in viral infection or replication on the host body. Main protease (M^{pro}) and Papain-like protease are two viral proteases that cause viral peptides to cleavage into functional units for virus

replication and packaging within the host cells. Hence anti-HIV drugs like lopinavir and ritonavir, have been explored. RdRp is the RNA-dependent RNA polymerase that is vital for viral RNA synthesis and may be blocked by existing antiviral drugs like Remdisivir¹¹. The entry of viral Spike glycoprotein entering human cells *via* Angiotensin-Converting Enzyme-2 (ACE2) receptor and consequently allowing viral endocytosis points out its potential as a therapeutic target, hence the broad-spectrum antiviral drug, Arbidol can act as virus-host cell inhibitor for treating SARS-CoV-2^{12,13}.

The Transmembrane protease Serine 2 plays an important role in proteolytic processing of S protein, priming to the receptor ACE2 binding in human cells¹⁴ can act as a potential target, and it has been shown that camostat mesylate, a clinically approved TMPRSS2 inhibitor, was able to block SARS-CoV-2 entry to human cells¹⁴ **Table 1**.

TABLE 1: TARGET PROTEINS AND THEIR ROLES DURING THE VIRAL INFECTION PROCESS

Target protein	Full name	Role	Drug candidate
3CLpro	Main protease 3CLpro	proteolysis of viral polyprotein into functional units	Ritonavir ¹¹ , Lopinavir ¹¹
PLpro	papain-like protease PLpro	proteolysis of viral polyprotein into functional units	Ritonavir ¹¹ , Lopinavir ¹¹
RdRp	RNA-dependent RNA polymerase	replicating viral genome	Remdisivir ¹¹ , Ribavirin ¹⁵
S protein	Spike glycoprotein	binding to host cell receptor ACE2	Arbidol ^{12, 13}
TMPRSS2	Transmembrane protease, serine 2	primes S protein to facilitate its binding to ACE2	Camostat mesylate ¹⁴
ACE2	Angiotensin-converting enzyme 2	binds to viral S protein	Arbidol ^{12, 13}

Among all the key targets, we have chosen the main protease as our protein of interest, as this target could be therapeutically inhibited.

Main Protease: In the Protein data bank, 396 X-ray and 3 NMR structures (Till 31st Oct 2020) are available related to SARS-CoV-2, amongst them, 200 structures are main protease target protein either complexed with a ligand or in apo form.¹⁶ Main protease architecture comprises of Domain1 (residues 8-101), Domain2 (residues 102-184), and Domain3 (residues 201-303). Domain 1 of both monomers is folded as a β -barrel, whereas Domain 2 of both monomers is folded in β -sheets¹⁷. The domain 3 is connected to domain 2 *via* a long loop in each monomer. The active site is surrounded by domains 1 and 2 with inhibitor placed inside. The analysis also shows the binding pocket of the protein is electrically neutral as it has a similar number of hydrophilic and hydrophobic residues. The crystal structural analysis points out some important residues like GLY 143, CYS 145, HIS 41, THR 25, MET 165 HIS 163. HIS 164, GLU 166, and GLN 189 in making H-bonds and hydrophobic interactions with the ligands^{18, 19}.

To select the 3D structure of the target, we analyzed all the available X-ray crystal structures, and finally based on its high resolution (1.31 Å), and the co-crystallized ligand poses that are nearby the catalytic dyad of CYS 145 and HIS 41. Also, the co-crystallized ligand for our selected PDB structure was very small, and hence we thought of exploring vital pharmacophoric features that could potentially favour good binding. We choose the reported co-crystallized structures, PDB ID: 5R82²⁰, and performed the SiteMap analysis using the Glide module²¹. The purpose of doing the SiteMap was to explore the active site of the main protease as well as to use the entire site points for our docking strategy that might have been missed if we had taken co-crystallized ligand for our grid

generation. Based on the D score and Site score we obtained a putative binding site that can be utilized for screening the drug bank database to find potential SARS-CoV-2 inhibitors. We also docked FDA approved drugs Lopinavir and Ritonavir¹¹ as standard for comparison with the database molecules. From this database, we included all the types of molecules having investigational, approved, and experimental status. The drug bank database²² compounds were docked using XP docking of the Glide module, followed by rescoring by free energy calculations. Based on the docking scores, interactions, pose and MM-GBSA results we selected three molecules, which were later studied and analysed using molecular dynamics (MD) simulations.

MATERIALS AND METHODS: Various calculations were carried out using the Schrodinger. We utilized the SARS-CoV-2 main protease co-crystallized structure (PDB ID: 5R82) from Protein Data Bank for our study¹⁶.

SiteMap Analysis: The protein target was subjected to SiteMap analysis to find the putative binding site. All the default parameters were used to obtain probable druggable sites based on D score and site scores. SiteMap²³ analyses the characteristic features of binding sites by the intensive search that results in the identification of regions that may facilitate binding of a ligand to the receptor. Hydrophobic and hydrophilic maps are generated; the latter is further divided into donor, acceptor, and metal-binding regions. Each site is assessed by calculation of SiteScore that includes physical parameters like volume, site size, exposure/enclosure hydrophilic, hydrogen bond donor/acceptor, etc. Generally, a good SiteScore of a binding site is 1.0. SiteScore, ranks the site with the highest score determines the drug ability. SiteMap uses an algorithm analogous to the Goodford's GRID algorithm, which uses

interaction energies between the protein and grid probes to locate energetically favourable sites. Sites were kept to be comprised of at least 15 site points²³. A restrictive hydrophobicity definition, a standard grid (1.0 Å), and the OPLS-3e force field was used (default settings in SiteMap).

Protein and Ligand Preparation: Protein was prepared in protein preparation wizard,²⁴ hydrogen atoms were added, and water molecules beyond 5 Å of the binding site were removed. Side-chains and loops were built using the prime module. All atomic charges and atom types were assigned. The energy minimization and refinement of the structure was done by using the OPLS-3e force field. The optimized target protein was later employed for docking studies. All the ligands from Drug-bank²² were prepared using the Ligprep wizard²⁵. The default parameters included: Ionizers, generating tautomers, generating possible conformers at pH 7 with OPLS-3e force field, thereby achieving the correct protonated state for each ligand used.

Receptor Grid Generation: Before docking, receptor grid generation is an essential step. The Centroid of the residues, predicted by SiteMap was defined as the grid box (15 Å) also default parameters like Van der Waals scaling factor 1.00, charge partial cut-off 0.25 and, OPLS-3e force field were used for grid generation.

Molecular Docking Studies: The ligands prepared by Ligprep were docked into the active sites of the main protease using the "extra-precision" (XP) mode of the Glide²¹ docking program (Maestro). This protocol facilitates docking by ligand flexibility and generation of multiple conformers within the rigid receptor. The Ligand interaction diagrams were used to understand the interactions between the ligand and the target. And the best conformation for each ligand was chosen based on

the better glide score (XP Gscore). Ligands that form hydrogen bonds with at least one active site of the target protein with good binding affinity analyses the final Gscore.

Rescoring using Prime MM-GBSA: The Binding affinity of the ligand with the receptor was further estimated using Prime MM-GBSA.²⁶ By applying OPLS-3e force field and generalized-Born surface area (GBSA) continuum solvent model, the binding free energy of the docked pose²⁷ was calculated with:

$$\Delta G_{\text{bind}} = G(\text{PL}) - G(\text{P}) - G(\text{L})$$

PL = protein-ligand complex P = Protein, L = Ligand.

Molecular Dynamics Simulations: MD simulations for protein-ligand complexes were performed using the Desmond package.²⁸ The OPLS3e force field was used to model the protein interactions, and the SPC mode was used for water molecules. Long-range electrostatic interactions were calculated using the Particle-mesh Ewald (PME) method with a grid spacing of 0.8 Å. Nose-Hoover thermostatic was used for maintaining the constant temperature and the Martina-Tobias-Klein method was used for the constant pressure. Periodic boundary conditions (PBC) were applied. After minimization, all the complexes were subjected to the production run for 20 ns in the NPT ensemble.

RESULTS AND DISCUSSION:

Site Map Analysis: The target protein binding site was predicted using the Site Map module. This gave us putative sites that we require for the docking studies. The results showed 2 sites out of 5, which were potentially druggable, as given in **Table 2**. Site 1 with the best score was selected for our docking study. Also, this site was the same site where the co-crystallized ligand was placed in the co-crystallized protein structure **Fig. 2, Table 2**.

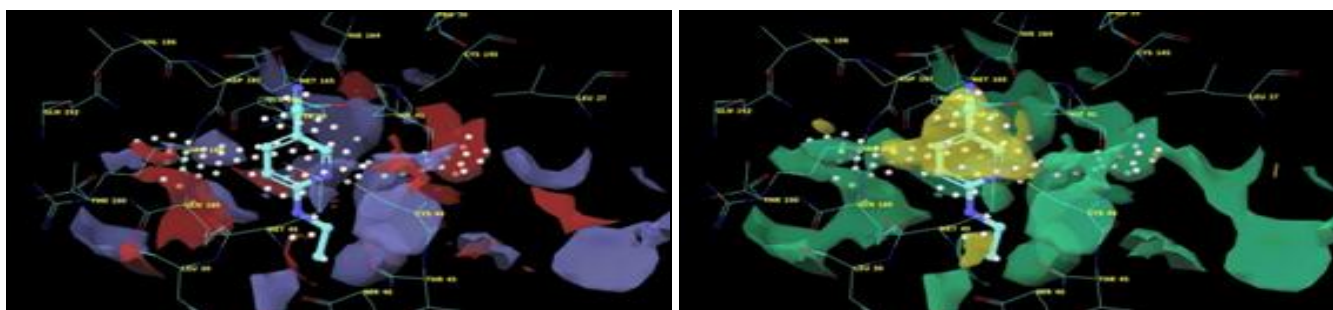


FIG. 2: SITE 1 AND CO-CRYSTALLIZED LIGAND SUPERIMPOSED. THE LEFT IMAGE REPRESENTS THE HYDROPHILIC SITES ENCLOSING THE ACTIVE SITE AND THE RIGHT IMAGE REPRESENTS THE HYDROPHOBIC SITES

TABLE 2: SITE MAP SCORES FOR 5R82

Site No.	Site Score	D Score
1	0.998	1.021
2	0.994	1.019
3	0.815	0.683
4	0.694	0.632
5	0.571	0.553

Site 1 is comprised of hydrophobic and hydrophilic areas **Fig. 2**. The entire area of Site 1 needs to occupy to get optimum binding. The co-crystallized ligand does not occupy the entire site, hence using our study we need to design molecules that would occupy the sites completely. Analyzing Site 1, it is seen that it has hydrophobic residues (represented by green colour in **Fig. 2, right**) like PHE140, LEU141, CYS 145, MET 49, MET 165, hydrophilic residues (represented by red and violet colour in **Fig. 2, left**) like ASN 142, SER 144, HIS 41, THR 26, THR 25, THR 24, GLN 189, HIS 163, HIS 164, negatively charged (GLU 166, ASP 187)

and positively charged residue (ARG 188) with a water molecule nearby (HOH 1171).

Molecular Docking: The docking protocol was validated as the redocking of the co-crystallized ligand showed the same interactions with the target protein. 8696 molecules were screened based on the similarity search on the Drug bank database which was docked into the binding site. **Table 3** contains the docking scores, Glide emodel, Glide energy and, MM-GBSA scores of the top 60 selected compounds. These 60 molecules were basically divided based on their status of approval, namely experimental, investigational, and approved molecules, and also they were chemically diverse in nature. Scores of the top 200 molecules are provided in **Supplementary Table S1**. Also, as a standard drug for reference, we used Ritonavir and Lopinavir in our study.

TABLE 3: SCORES OF SELECTED TOP 60 MOLECULES FROM DRUG BANK DATABASE DOCKED ON 5R82

S. no	Status	Chemical ID	XP G Score	Glide emodel (kcal/mol)	Glide energy (kcal/mol)	MMGBSA dG Bind (kcal/mol)
	Co-crystallized ligand	-	-4.555	-34.306	-27.50	-51.40
Approved						
1	approved	DB09135	-9.788	-59.915	-52.346	-58.88
2	approved	DB00841	-8.907	-53.824	-43.121	-56.32
3	approved	DB06814	-8.702	-55.798	-43.299	-45.8
4	approved	DB01095	-8.47	-61.467	-44.442	-63.3
5	approved	DB11263	-8.429	-55.713	-44.754	-59.07
6	approved; experimental; investigational	DB04465	-8.409	-40.385	-35.039	-47.62
7	approved	DB00399	-8.404	-47.31	-40.975	-28.43
8	approved	DB00598	-8.331	-53.858	-46.702	-56.28
9	approved; investigational	DB01133	-8.306	-52.804	-44.212	-54.70
10	approved	DB01098	-7.993	-58.149	-49.931	-71.40
11	approved	DB09477	-7.615	-52.718	-47.002	-48.09
12	approved; investigational	DB13074	-7.603	-75.919	-50.131	-53.73
13	approved; investigational	DB03247	-7.454	-53.482	-46.911	-46.02
14	approved	DB00876	-7.054	-49.144	-43.837	-60.36
15	approved	DB11185	-6.992	-47.23	-39.441	-42.25
16	approved; investigational; nutraceutical	DB00131	-6.956	-50.014	-46.301	-17.89
17	approved; investigational	DB06603	-6.904	-56.276	-41.47	-59.44
18	approved; investigational	DB01415	-6.81	-61.315	-51.305	-60.08
19	approved	DB00415	-6.63	-47.492	-38.559	-39.30
20	approved	DB00973	-6.582	-55.129	-40.357	-46.22
Investigational						
1	investigational	DB04983	-10.296	-75.015	-72.076	-65.17
2	investigational	DB12116	-9.157	-63.806	-53.35	-69.45
3	investigational	DB15246	-8.984	-74.001	-54.55	-55.39
4	investigational	DB05779	-8.739	-55.58	-46.168	-50.88
5	investigational	DB06548	-8.621	-53.23	-40.882	-40.29
6	investigational	DB12039	-8.016	-42.046	-38.057	-42.30
7	investigational	DB05255	-7.788	-57.049	-49.78	-70.39
8	investigational	DB13084	-7.781	-59.684	-44.017	-65.44
9	investigational	DB11711	-7.658	-60.963	-51.443	-71.67

10	investigational	DB06309	-7.567	-55.6	-46.905	-62.67
11	investigational	DB12795	-7.436	-52.857	-45.264	-72.92
12	investigational	DB04882	-7.294	-52.579	-50.467	-57.86
13	investigational	DB12708	-7.171	-63.891	-50.699	-72.05
14	investigational	DB11656	-7.106	-58.418	-45.787	-64.43
15	investigational	DB12080	-6.975	-49.898	-38.051	-59.55
16	investigational	DB05553	-6.88	-69.49	-54.589	-61.87
17	investigational	DB11676	-6.821	-43.889	-37.318	-32.64
18	investigational; nutraceutical	DB04789	-6.807	-64.359	-52.447	-46.69
19	investigational	DB12760	-6.702	-57.253	-42.997	-56.40
20	investigational	DB13019	-6.671	-62.989	-49.581	-71.63
Experimental						
1	experimental	DB04226	-11.717	-59.777	-49.449	-53.20
2	experimental	DB02485	-11.1	-69.373	-64.572	-36.88
3	experimental	DB03962	-10.81	-71.655	-70.655	-69.07
4	experimental	DB03973	-10.257	-61.978	-52.585	-52.70
5	experimental	DB01713	-10.136	-67.771	-57.858	-65.15
6	experimental	DB04099	-10.055	-77.101	-59.153	-46.05
7	experimental	DB01687	-10.042	-46.521	-38.458	-44.84
8	experimental	DB08237	-9.7	-80.979	-54.248	-70.23
9	experimental	DB03543	-9.678	-59.762	-51.402	-53.53
10	experimental; investigational	DB01633	-9.651	-51.368	-43.597	-62.05
11	experimental	DB02338	-9.5	-93.72	-65.62	-62.59
12	experimental	DB04143	-9.497	-51.659	-42.303	-45.76
13	experimental	DB01697	-9.422	-52.846	-50.229	-58.03
14	experimental	DB04176	-9.183	-49.931	-44.015	-39.54
15	experimental	DB04514	-9.14	-71.024	-59.635	-62.45
16	experimental	DB02819	-9.096	-44.815	-37.233	-59.76
17	experimental	DB14128	-9.043	-63.215	-58.106	-51.41
18	experimental	DB02675	-8.894	-56.268	-42.555	-54.58
19	experimental	DB02790	-8.696	-61.645	-59.084	-50.78
20	experimental	DB02319	-8.556	-87.081	-66.698	-35.41
Standard						
1	approved	Ritonavir	-6.225	-72.386	-55.698	-52.83
2	approved	Lopinavir	-6.108	-47.867	-38.974	-40.35

SUPPLEMENTARY TABLE S1: TOP 200 MOLECULES DOCKING SCORES AND MM-GBSA ENERGY VALUES

S. no.	Status	Chemical ID	XP GScore	Glide emodel (kcal/mol)	Glide energy (kcal/mol)	MMGBSA dG Bind (kcal/mol)
1	experimental	DB04226	-11.717	-59.777	-49.449	-53.2
2	experimental	DB02485	-11.1	-69.373	-64.572	-36.88
3	experimental	DB03962	-10.81	-71.655	-70.655	-69.07
4	investigational	DB04983	-10.296	-75.015	-72.076	-65.17
5	experimental	DB03973	-10.257	-61.978	-52.585	-52.7
6	experimental	DB01713	-10.136	-67.771	-57.858	-65.15
7	experimental	DB04099	-10.055	-77.101	-59.153	-46.05
8	experimental	DB01687	-10.042	-46.521	-38.458	-44.84
9	approved	DB09135	-9.788	-59.915	-52.346	-58.88
10	experimental	DB08237	-9.7	-80.979	-54.248	-70.23
11	experimental	DB03543	-9.678	-59.762	-51.402	-53.53
12	experimental; investigational	DB01633	-9.651	-51.368	-43.597	-62.05
13	experimental	DB02338	-9.5	-93.72	-65.62	-62.59
14	experimental	DB04143	-9.497	-51.659	-42.303	-45.76
15	experimental	DB01697	-9.422	-52.846	-50.229	-58.03
16	experimental	DB04176	-9.183	-49.931	-44.015	-39.54
17	investigational	DB12116	-9.157	-63.806	-53.35	-69.45
18	experimental	DB04514	-9.14	-71.024	-59.635	-62.45
19	experimental	DB02819	-9.096	-44.815	-37.233	-59.76
20	experimental	DB14128	-9.043	-63.215	-58.106	-51.41

21	investigational	DB15246	-8.984	-74.001	-54.55	-55.39
22	approved	DB00841	-8.907	-53.824	-43.121	-56.32
23	experimental	DB02675	-8.894	-56.268	-42.555	-54.58
24	investigational	DB05779	-8.739	-55.58	-46.168	-50.88
25	approved; vet_approved	DB06814	-8.702	-55.798	-43.299	-45.8
26	experimental	DB02790	-8.696	-61.645	-59.084	-50.78
27	investigational	DB06548	-8.621	-53.23	-40.882	-40.29
28	experimental	DB02319	-8.556	-87.081	-66.698	-35.41
29	experimental	DB02557	-8.501	-64.541	-53.001	-50.84
30	approved	DB01095	-8.47	-61.467	-44.442	-63.3
31	approved	DB11263	-8.429	-55.713	-44.754	-59.07
32	approved; experimental; investigational	DB04465	-8.409	-40.385	-35.039	-47.62
33	approved	DB00399	-8.404	-47.31	-40.975	-28.43
34	experimental	DB08116	-8.396	-74.402	-52.619	-37.03
35	experimental	DB06928	-8.357	-52.223	-41.984	-58.69
36	experimental	DB04395	-8.347	-57.979	-51.691	-43.25
37	approved	DB00598	-8.331	-53.858	-46.702	-56.28
38	approved; investigational; vet_approved	DB01133	-8.306	-52.804	-44.212	-54.7
39	experimental	DB04762	-8.296	-64.708	-54.944	-57.6
40	experimental	DB07651	-8.191	-72.017	-52.03	-62.49
41	experimental	DB03161	-8.166	-58.339	-50.658	-48.21
42	experimental	DB04495	-8.143	-77.165	-61.21	-71.84
43	experimental	DB14210	-8.136	-65.557	-52.66	-51.52
44	experimental	DB04158	-8.099	-72.051	-65.142	-48.69
45	experimental	DB03573	-8.096	-54.533	-43.296	-55.5
46	experimental	DB14217	-8.09	-61.997	-44.114	-59.04
47	experimental	DB04778	-8.08	-59.44	-46.137	-36.8
48	investigational	DB12039	-8.016	-42.046	-38.057	-42.3
49	experimental	DB03576	-8	-51.995	-44.411	-45.12
50	approved	DB01098	-7.993	-58.149	-49.931	-71.4
51	experimental	DB02358	-7.99	-77.146	-60.199	-54.74
52	experimental	DB01908	-7.99	-67.006	-56.961	-74.85
53	experimental	DB02908	-7.974	-46.21	-38.958	-39.85
54	experimental	DB02375	-7.965	-46.158	-41.904	-51.03
55	experimental	DB08500	-7.949	-42.021	-39.196	-57.66
56	experimental	DB04750	-7.941	-51.716	-46.941	-57.16
57	experimental	DB02023	-7.919	-53.5	-44.062	-35.1
58	experimental	DB03577	-7.811	-53.6	-42.217	-47.05
59	experimental	DB03067	-7.803	-84.517	-57.891	-75.81
60	experimental	DB04190	-7.796	-79.635	-58.327	-85.3
61	investigational	DB05255	-7.788	-57.049	-49.78	-70.39
62	investigational	DB13084	-7.781	-59.684	-44.017	-65.44
63	experimental	DB01690	-7.701	-81.097	-70.107	-31.74
64	experimental	DB03591	-7.694	-71.868	-55.426	-72.39
65	experimental	DB03227	-7.694	-53.258	-48.116	-52.16
66	investigational	DB11711	-7.658	-60.963	-51.443	-71.67
67	experimental	DB03691	-7.654	-56.296	-46.897	-50.9
68	experimental	DB01678	-7.649	-74.824	-58.016	-69.02
69	experimental	DB02943	-7.636	-68.621	-57.541	-64.16
70	experimental	DB13540	-7.621	-50.045	-45.246	-53.03
71	approved	DB09477	-7.615	-52.718	-47.002	-48.09
72	experimental	DB02307	-7.604	-63.677	-51.761	-65.88
73	approved; investigational	DB13074	-7.603	-75.919	-50.131	-53.73
74	investigational	DB06309	-7.567	-55.6	-46.905	-62.67

75	experimental	DB04649	-7.511	-65.715	-52.109	-55.39
76	experimental	DB03325	-7.505	-65.579	-56.379	-49.33
77	experimental	DB04437	-7.503	-52.529	-45.128	-55.44
78	experimental; investigational	DB04216	-7.496	-46.768	-41.024	-46.11
79	experimental	DB02742	-7.491	-47.307	-35.327	-35.16
80	experimental	DB08230	-7.46	-49.23	-40.669	-43.92
81	approved; investigational	DB03247	-7.454	-53.482	-46.911	-46.02
82	investigational	DB12795	-7.436	-52.857	-45.264	-72.92
83	experimental	DB04328	-7.411	-38.316	-35.443	-30.51
84	experimental	DB04301	-7.367	-45.637	-42.155	-21.33
85	experimental	DB04200	-7.363	-56.544	-41.992	-63.83
86	experimental	DB04133	-7.349	-62.35	-45.822	-56.61
87	experimental	DB07963	-7.345	-57.131	-44.011	-58.61
88	experimental	DB08731	-7.335	-64.397	-49.529	-59.67
89	experimental	DB04662	-7.317	-54.26	-40.921	-53.2
90	experimental	DB07795	-7.308	-44.998	-40.494	-44.04
91	investigational	DB04882	-7.294	-52.579	-50.467	-57.86
92	experimental	DB07589	-7.294	-64.813	-53.34	-62.97
93	experimental	DB03846	-7.289	-56.992	-48.292	-45.87
94	experimental	DB08613	-7.287	-60.837	-45.845	-60.19
95	experimental	DB04411	-7.286	-46.053	-35.981	-42.17
96	experimental	DB08272	-7.284	-48.282	-40.888	-50.29
97	experimental	DB07448	-7.279	-58.167	-44.802	-38.03
98	experimental	DB02154	-7.274	-54.123	-46.942	-42.86
99	experimental	DB02360	-7.266	-56.676	-43.545	-52.95
100	experimental	DB04656	-7.239	-50.458	-39.759	-50.09
101	experimental	DB07676	-7.232	-59.944	-43.519	-57.73
102	experimental	DB04632	-7.202	-69.827	-47.062	-63.06
103	experimental	DB14127	-7.186	-63.314	-52.857	-75.71
104	experimental	DB04042	-7.171	-66.328	-58.364	-68.32
105	investigational	DB12708	-7.171	-63.891	-50.699	-72.05
106	experimental	DB06984	-7.161	-42.449	-32.77	-51.44
107	experimental	DB08485	-7.155	-47.737	-40.746	-52.92
108	experimental	DB08240	-7.142	-57.626	-41.822	-58.43
109	experimental	DB07837	-7.123	-53.225	-43.975	-59.56
110	investigational	DB11656	-7.106	-58.418	-45.787	-64.43
111	experimental	DB02450	-7.102	-51.591	-45.784	-54.9
112	experimental	DB03097	-7.095	-65.163	-50.573	-58.41
113	experimental	DB01734	-7.076	-48.771	-39.915	-33.89
114	vet_approved	DB11541	-7.059	-50.179	-39.161	-46.52
115	approved	DB00876	-7.054	-49.144	-43.837	-60.36
116	experimental	DB08264	-7.032	-31.09	-26.631	-43.65
117	experimental	DB07783	-7.021	-66.326	-51.404	-58.51
118	approved	DB11185	-6.992	-47.23	-39.441	-42.25
119	investigational	DB12080	-6.975	-49.898	-38.051	-59.55
120	approved; investigational;	DB00131	-6.956	-50.014	-46.301	-17.89
121	nutraceutical experimental	DB03525	-6.955	-42.398	-35.545	-51.96
122	experimental; investigational	DB11737	-6.953	-55.539	-45.432	-55.65
123	experimental	DB07587	-6.952	-63.551	-45.982	-65.49
124	experimental	DB08366	-6.936	-57.404	-41.877	-40.3
125	experimental	DB08702	-6.935	-56.955	-45.045	-51.32
126	experimental	DB01771	-6.905	-50.716	-41.39	-59.87
127	approved; investigational	DB06603	-6.904	-56.276	-41.47	-59.44
128	experimental	DB02511	-6.901	-62.086	-48.756	-53.44

129	experimental	DB07890	-6.891	-49.491	-41.698	-52.9
130	experimental	DB02862	-6.88	-38.493	-34.488	-45.01
131	investigational	DB05553	-6.88	-69.49	-54.589	-61.87
132	experimental	DB03171	-6.88	-48.87	-41.401	-48.39
133	experimental	DB03804	-6.869	-49.763	-43.071	-63.08
134	experimental	DB07756	-6.852	-50.248	-41.796	-53.76
135	experimental	DB08392	-6.847	-56.217	-48.374	-55.94
136	experimental	DB07550	-6.844	-61.859	-44.492	-64.96
137	experimental	DB04175	-6.829	-42.933	-37.275	-51.92
138	experimental; vet_approved	DB11396	-6.828	-46.816	-37.458	-57.31
139	investigational	DB11676	-6.821	-43.889	-37.318	-32.64
140	approved; investigational	DB01415	-6.81	-61.315	-51.305	-60.08
141	investigational; nutraceutical	DB04789	-6.807	-64.359	-52.447	-46.69
142	experimental	DB07484	-6.801	-40.122	-39.346	-43.38
143	experimental	DB14209	-6.79	-50.655	-40.102	-56.58
144	experimental	DB13781	-6.786	-56.893	-46.432	-59.02
145	experimental	DB03314	-6.785	-40.232	-32.999	-42.17
146	experimental	DB07520	-6.782	-57.342	-44.045	-49.83
147	experimental	DB08399	-6.776	-39.829	-33.034	-46.7
148	experimental	DB02662	-6.763	-44.239	-37.874	-37.16
149	experimental	DB04187	-6.762	-60.64	-46.839	-65.63
150	experimental	DB03679	-6.76	-40.379	-33.622	-49.22
151	experimental	DB07663	-6.747	-60.921	-46.138	-59.85
152	experimental	DB04285	-6.726	-58.204	-52.92	-71.64
153	experimental	DB06980	-6.717	-36.558	-29.628	-49.04
154	experimental	DB07185	-6.716	-54.706	-41.621	-53.13
155	experimental	DB03835	-6.708	-48.621	-41.082	-50.1
156	investigational	DB12760	-6.702	-57.253	-42.997	-56.4
157	experimental	DB03012	-6.699	-43.935	-39.055	-31.89
158	experimental	DB01852	-6.695	-41.224	-38.863	-44.91
159	experimental	DB04582	-6.682	-48.649	-41.863	-54.63
160	experimental	DB06981	-6.672	-33.061	-28.868	-48.04
161	investigational	DB13019	-6.671	-62.989	-49.581	-71.63
162	experimental	DB04641	-6.658	-35.273	-30.003	-29.69
163	investigational	DB13027	-6.657	-49.241	-40.87	-47.71
164	experimental	DB13596	-6.644	-41.906	-33.628	-43.85
165	approved; vet_approved	DB00415	-6.63	-47.492	-38.559	-39.3
166	investigational	DB06620	-6.609	-53.015	-37.635	-46.05
167	experimental	DB07105	-6.605	-65.632	-50.551	-70.66
168	experimental	DB08395	-6.6	-55.286	-47.274	-58.81
169	experimental	DB07649	-6.585	-53.737	-43.169	-61.2
170	approved	DB00973	-6.582	-55.129	-40.357	-46.22
171	experimental	DB02830	-6.564	-64.793	-47.861	-57.27
172	approved; vet_approved	DB00584	-6.563	-57.618	-43.607	-55.23
173	experimental	DB07543	-6.56	-45.175	-37.611	-52.42
174	investigational	DB13039	-6.559	-43.181	-35.708	-55.69
175	experimental	DB04001	-6.556	-50.167	-36.701	-32.02
176	approved	DB13166	-6.55	-70.104	-51.66	-78.61
177	experimental	DB13660	-6.544	-55.718	-43.767	-66.48
178	experimental	DB07047	-6.529	-46.075	-34.831	-55.51
179	approved; investigational	DB01328	-6.525	-67.807	-54.401	-69.13
180	experimental; nutraceutical	DB14732	-6.504	-51.274	-39.34	-35.66
181	experimental	DB07527	-6.503	-52.924	-44.892	-38.95

182	experimental	DB07680	-6.503	-59.077	-45.986	-52.83
183	experimental	DB08735	-6.495	-38.231	-28.759	-61.27
184	experimental	DB04293	-6.492	-55.184	-41.117	-42.99
185	approved	DB11217	-6.486	-40.048	-35.314	-38.1
186	experimental	DB04206	-6.485	-39.61	-32.546	-37.35
187	approved; investigational	DB13139	-6.485	-37.056	-32.677	-47.96
188	experimental	DB08251	-6.484	-54.504	-45.954	-52.84
189	experimental	DB02642	-6.481	-48.803	-35.757	-41.34
190	experimental	DB03628	-6.476	-38.897	-31.873	-28.96
191	investigational	DB06195	-6.472	-56.842	-45.433	-70.5
192	experimental	DB14663	-6.466	-59.616	-47.144	-39.14
193	experimental	DB07060	-6.465	-38.773	-31.711	-47.31
194	experimental	DB04623	-6.458	-59.033	-54.304	-51.8
195	investigational	DB05424	-6.458	-69.185	-52.871	-77.32
196	experimental	DB01925	-6.456	-29.458	-25.945	-36.84
197	experimental	DB01766	-6.443	-35.29	-32.283	-41.11
198	experimental	DB08111	-6.442	-49.019	-38.351	-51.65
199	experimental	DB07125	-6.44	-50.677	-41.371	-52.13
200	investigational	DB12072	-6.432	-55.302	-35.924	-56.59

All the molecules with good docking scores were analyzed and the XP Gscore of -6.4 kcal/mol was kept as minimum cut off (because we wanted to select only those molecules which had better scores than Ritonavir or Lopinavir) and -11.717 kcal/mol as the highest score. After analysing 200 molecules systematically, it was observed that HIS 41, GLU 166, GLN 189 as the most common H-bond interaction. As HIS 41 is a part of the catalytic dyad we were able to correlate that our screened molecules were docked near the catalytic site. Also, we found numerous hydrophobic interactions with MET 49, MET 165. As the docking scores alone were not enough to differentiate the molecules, we utilized glide emodel, and MM-GBSA based binding free energy (ΔG -bind), and binding poses for selecting the best complexes for MD simulations. The use of prime MM-GBSA was done for rescoring. All the selected complexes, after XP docking, were subjected to prime MM-GBSA calculations. MM-GBSA ΔG -bind scores for all the selected compounds are given in **Table 3**. The negative values of ΔG -bind indicate that the selected compounds favourably interact with the receptor. The ligand-binding energies for all the top 200 screened compounds are in the range of -17.89 kcal/mol to -85.3 kcal/mol. The binding energy for the co-crystallized inhibitor with SARS-CoV-2 main protease was -51.4 kcal/mol. The binding energies for three selected compounds (A,B,C) and two antivirals (D,E) are -53.2 kcal/mol, -65.88 kcal/mol, -65.15 kcal/mol, -52.83 kcal/mol and -40.35 kcal/mol respectively.

Thus indicating a better binding affinity of selected screened molecules compared to standard antivirals. Among the top hits from molecular docking calculations, DB04226 shows the best docking score (-11.717 kcal/mol), which is considerably higher than the co-crystallized inhibitor and standard approved protease inhibitors (Ritonavir and Lopinavir). Moreover, glide emodel scores correlate well with the MM-GBSA ΔG -bind values. These findings strongly suggest that the selected compounds may inhibit the SARS-CoV-2 main protease. All the 200 molecules belong to diverse chemical classes like dipeptides, nucleotides, nucleosides, glycosides, xanthenes, catechins. And among them dipeptides, nucleosides showed high docking scores. Thus giving us the idea that such molecules have a better pharmacophoric features to interact with the target residues. We are aware of the fact that the molecular docking study only reveals the static scenario of the ligand docked to the protein in one particular pose. Hence to validate this static pose, we performed a molecular dynamics study, where we could analyze the dynamics of the different poses of the complex within a particular timespan.

Therefore, from the 200 molecules analyzed, we took three molecules for further validation, DB02307 was selected as this molecule engulfed inside the active site in a complete manner and, also it could completely superimpose on the co-crystallized ligand (hence giving a good hint for better binding), DB04226 and DB01713 were

chosen mainly because of their good docking score and optimum binding energy compared to other molecules. Also, all these three molecules were chemically diverse in nature. To keep a standard for comparison, we took FDA-approved antiviral

main protease inhibitors Ritonavir, Lopinavir, and Co-crystallized ligand for our molecular dynamics study. The binding pose of the selected docked molecules is shown in **Fig. 3**.

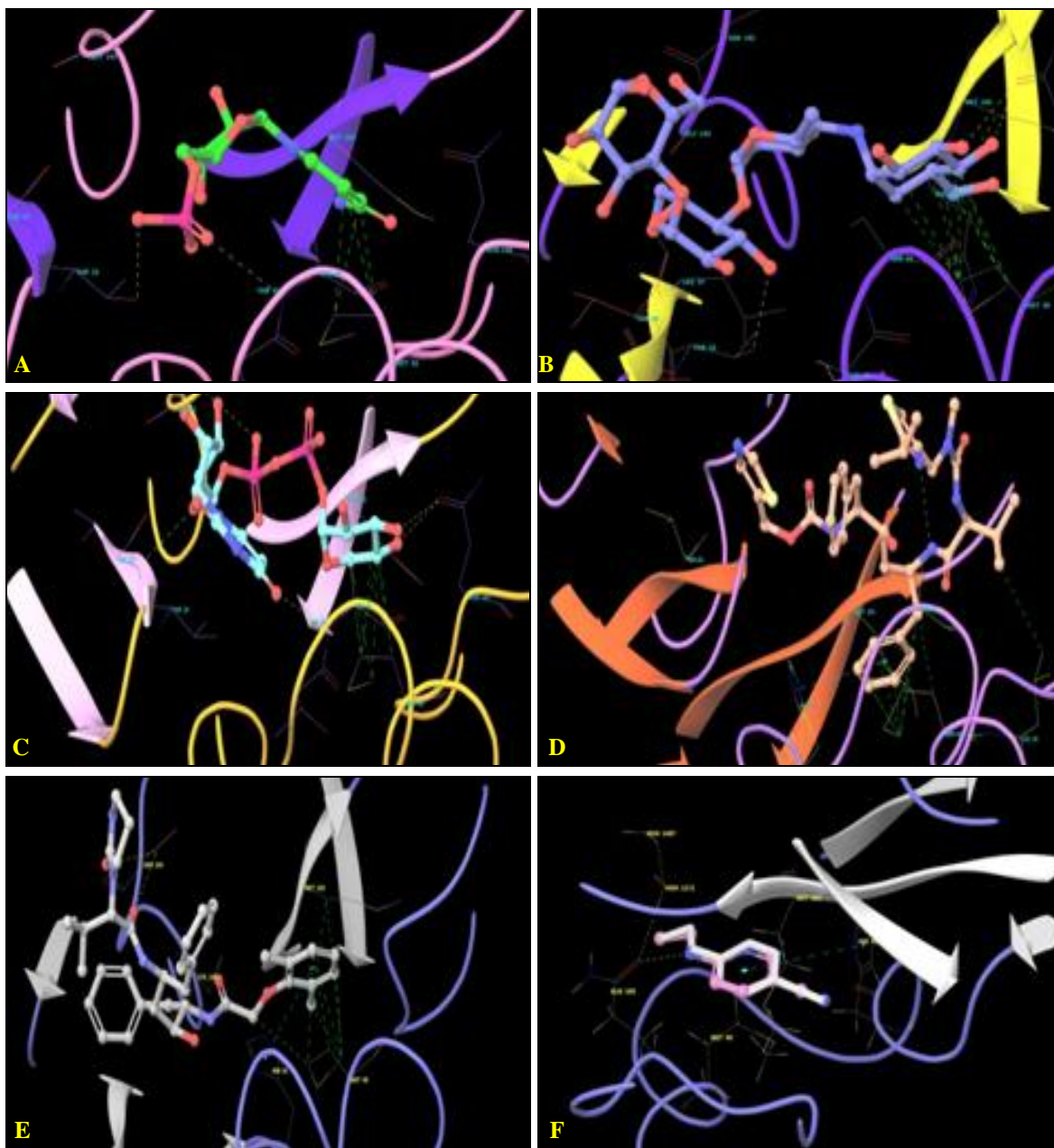


FIG. 3: BINDING MODES OF THREE SELECTED COMPLEXES DB02307 (A); DB04226 (B); DB01713 (C); RITONAVIR (D); LOPINAVIR (E) AND CO-CRYSTALLIZED LIGAND (F) ON 5R82

Molecular Dynamics Simulations: The backbone RMSD of the protein-ligand complex for all 6 molecules increased gradually then gets stable till 20 ns, **Fig. 4**. Low RMSD during the simulation indicates the stable complex formation. DB02307 shows excellent stability as this complex is equilibrated at 2 ns and remains stable throughout the simulation with the least conformational

changes **Fig. 4**. All three selected compounds, Ritonavir, Lopinavir, and co-crystallized ligand, remain stable throughout the simulation, with the change in backbone RMSD within the acceptable range of 1-3Å. As suggested via protein backbone RMSD, ligand RMSD was also found stable throughout the simulation with minimal fluctuation.

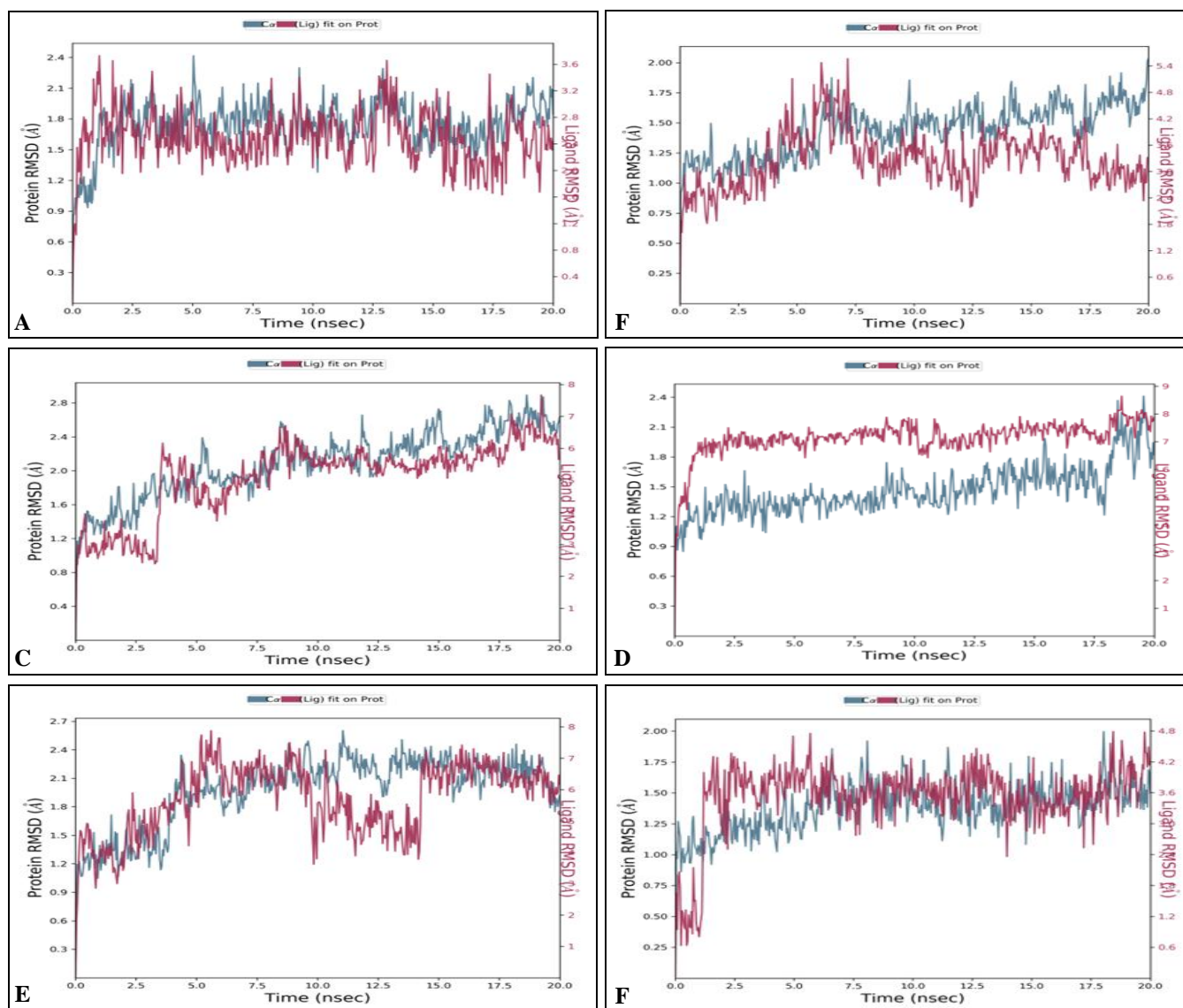


FIG. 4: RMSD OF PROTEIN AND LIGAND BACKBONES DURING THE SIMULATION DB02307 (A); DB04226 (B); DB01713 (C); RITONAVIR (D); LOPINAVIR (E); CO-CRYSTALLIZED LIGAND (F) ON 5R82

RMSF Analysis: This study gave us the overall picture of the protein environment when bound to the ligand, *i.e.* the fluctuations the residues undergo. The graphs in **Supplementary Fig. S1** show the fluctuations marked by peaks where the orange and sky blue colour areas represent the secondary structure. Generally, this area remains stable as compared to the loop regions; thus more peaks are seen in loop regions. The green colour depicts the residues which are having contacts with the ligand. The co-crystallized ligand with 5R82 undergo lesser fluctuations (0.4 – 0.8 Å) while interacting with HIS 41, MET 49, CYS 145, MET 165, GLU 166, and VAL 186 to GLN 189 region. Whereas the fluctuation increases to 1.1 Å for MET 49 interactions. Also there is a huge fluctuation (2.4 Å) in the region within residue 270 to 280. But this

region doesn't have any contact with ligand; hence it may not need much focus. Similarly, we analyzed all our top-scoring molecules and found out the fluctuations for important residues that are in contact with the ligand. (**Supplementary Fig. S1**) DB02307, DB01713, DB04226, and the two antivirals showed fluctuations in the range of 0.60 Å to 1.50 Å, where the ligands made contact with the protein. Interestingly higher fluctuation (2.0 Å - 2.2 Å) was observed for DB04226 near VAL 186 to GLN 192, thus indicating a slight fluctuation in this region due to ligand-protein contacts. This fluctuation was not observed in other graphs hence give us a clue that apart from HIS 41 and CYS 145, the region between residues 186 to 192 may also play a vital role in ligand-protein interactions (**Supplementary Fig. S1**).

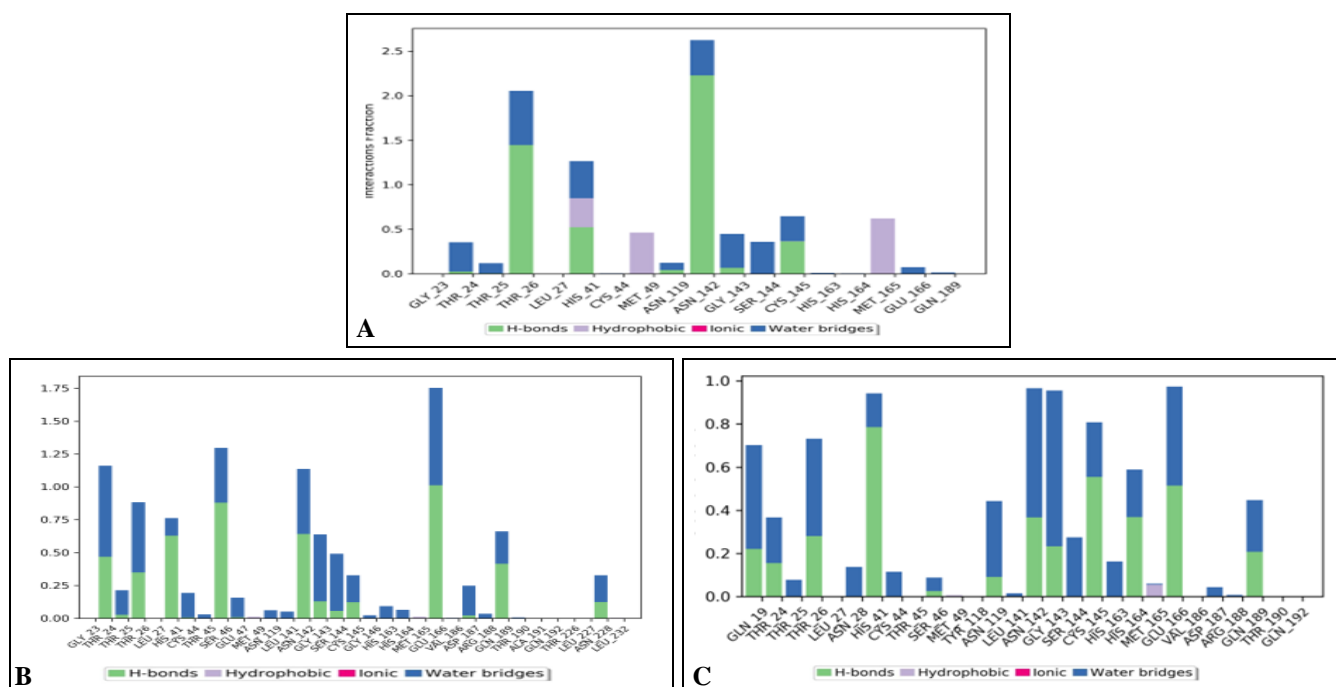
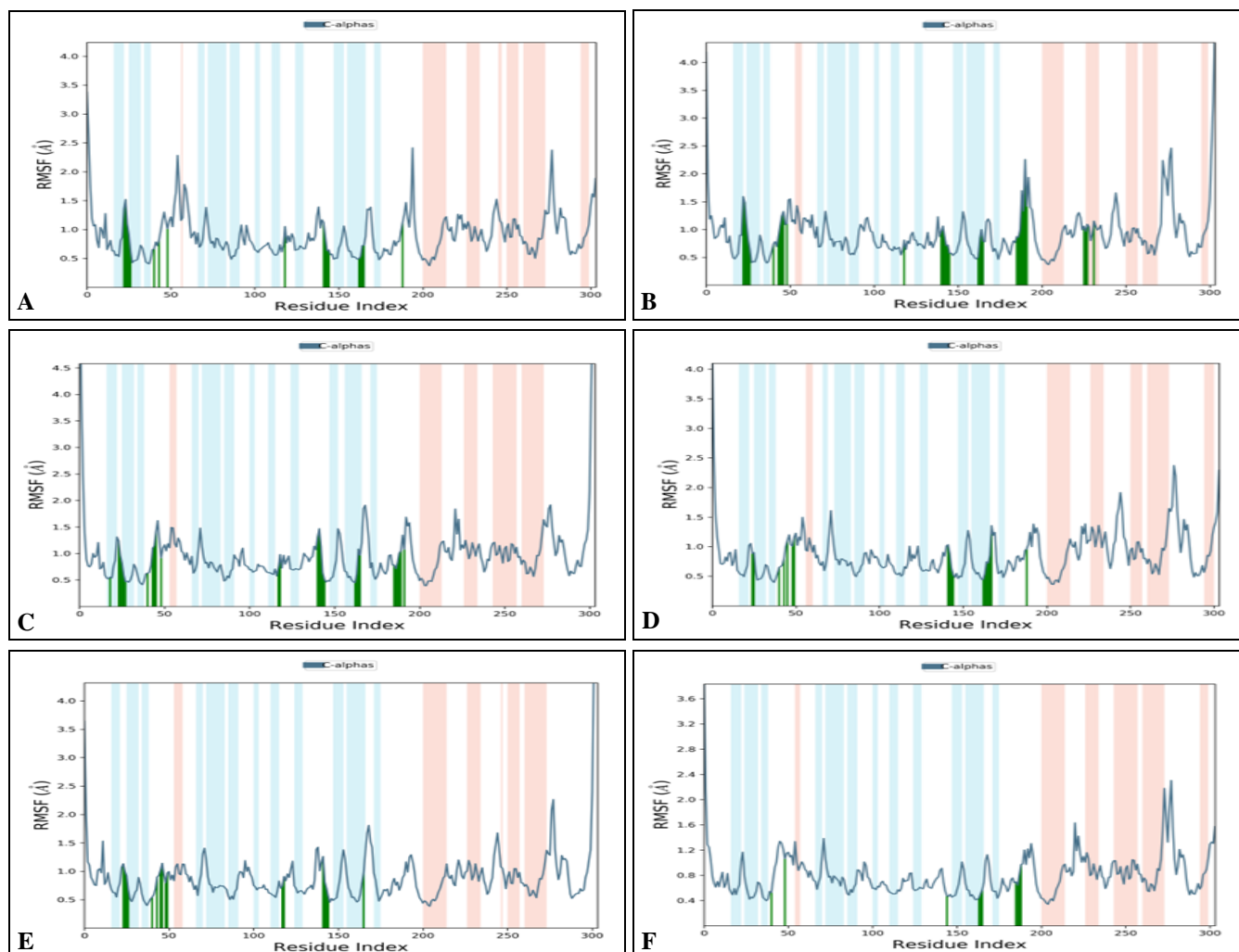


FIG. 5 (A); (B); (C): HISTOGRAM REPRESENTING THE H-BOND INTERACTIONS MAINTAINED DURING THE SIMULATION FOR DB02307 (LEFT); DB04226 (MIDDLE); DB01713 (RIGHT)



SUPPLEMENTARY FIG. S1: RMSF GRAPHS FOR DB02307 (A); DB04226 (B); DB01713 (C); RITONAVIR (D); LOPINAVIR (E); AND CO-CRYSTALLIZED LIGAND (F) DURING 20NS SIMULATION

H-bond Interaction and Interaction Stability

Analysis: To understand the stability of predicted protein-ligand complexes, we analyzed the hydrogen bond formation during the 20 ns simulation. DB02307 showed more than 100% interaction stability in H-bond interactions. This was observed since this molecule maintained three H-bond, two water bridges, and one hydrophobic interaction via THR 26, HIS 41, and ASN 142. Also, there was 70% stability for H-bond interaction with CYS 141, which is a part of the catalytic dyad of the main protease. **Fig. 5(a)** DB04226 showed H-bond interactions with the main catalytic residues, namely HIS 41 and CYS 145 along with other important nearby residues in the active site. High interaction stability was observed in ASN 142, THR 24, THR 26, GLU 166, and GLN 189 with a fraction of water bridge interaction and H-bond interactions. Also, the

graph shows that interaction stability for HIS 41 and CYS 145 was in the range of 75% to 30%. **Fig. 6 (b) DB01713** analysis showed that GLU 166 and ASN 142 had near to 90% interaction stability for H-bond interaction with some fraction of water bridge interaction. For DB02307, ASN 142 shows approximately 260% stability in interaction **Fig. 5a** and almost 220% stability for H-bond stability during the simulation. **Fig. 6a** shows the breakage of this total fraction into 3 parts, where the same residue interacts with three different ligand points with 64%, 74%, and 79%. The 2D ligand-protein interactions diagram gives detailed information about the interaction fractions. For DB04226, SER 46, HIS 41 showed H-bond interaction stability near 60%; GLU 166 showed 71% H-bond interaction stability **Fig. 6(a), (b), (c)** also GLY 143 showed water-mediated interaction.

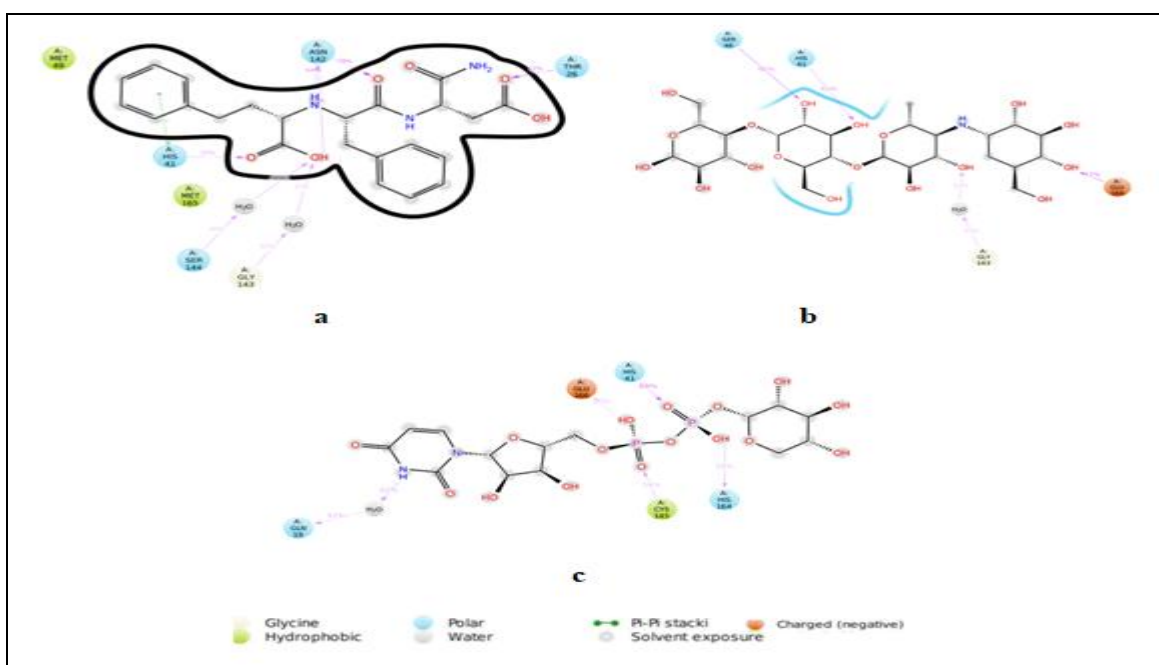
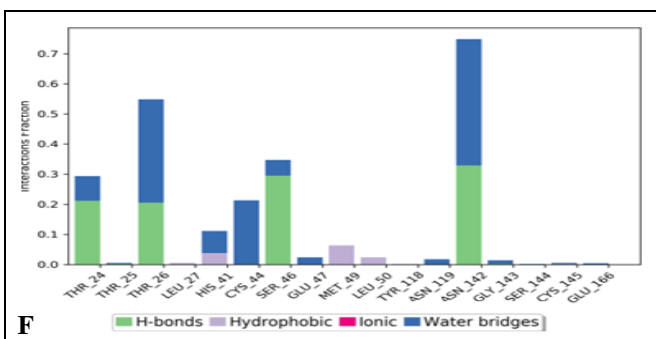
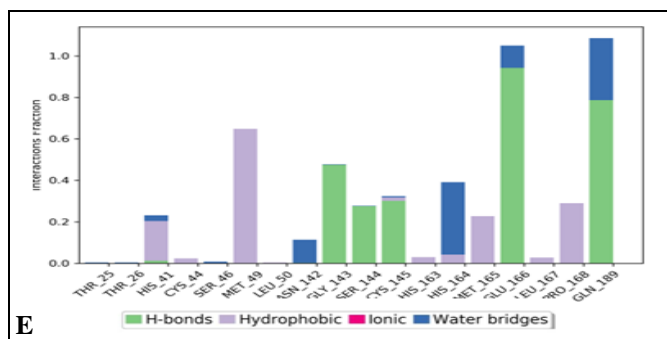


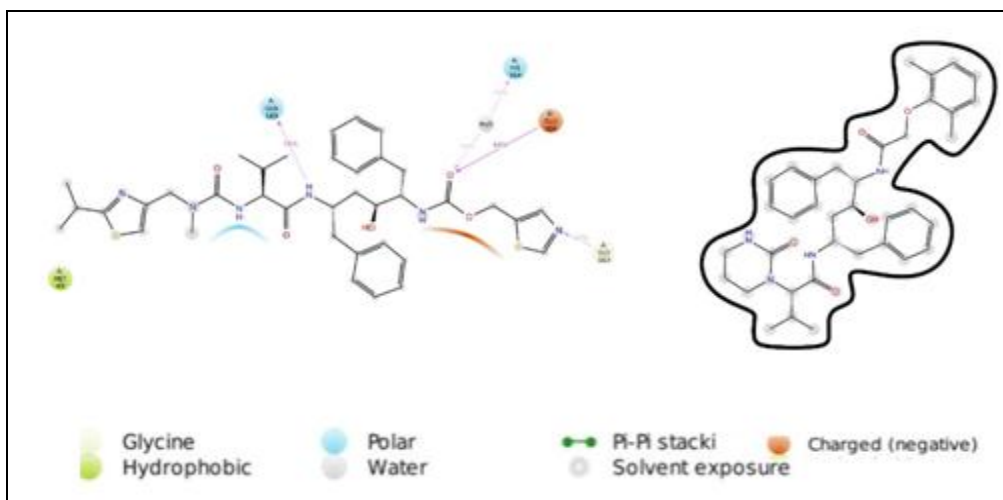
FIG. 6 (A); (B); (C): LIGAND PROTEIN CONTACT 2D DIAGRAM FOR DB02307 (LEFT); DB04226 (MIDDLE); DB01713 (RIGHT)



SUPPLEMENTARY FIG. S2 (A); (B): HISTOGRAM REPRESENTING THE H-BOND INTERACTIONS MAINTAINED DURING THE SIMULATION FOR RITONAVIR (LEFT) AND LOPINAVIR (RIGHT)

Along with the selected molecules, we also performed this analysis for Ritonavir and Lopinavir. Ritonavir showed stability in H-bond interaction *via* GLU 166 and GLN 189 with nearby 100% stability. Also, some hydrophobic interactions are observed for MET 49 with 70% stability. **Supplementary Fig. S2 (a), (b)** However, Lopinavir showed no stable contacts in the Ligand protein contact plot **Supplementary Fig. S3(b)**, but in the histogram, there were some residues like ASN 142, THR 24, THR 26 that showed interaction stability in the range of 30% to 70%.

Supplementary Fig. S3 (a) It is quite evident that as the docking deals with the static environment of the protein compared to the dynamic nature in simulation study, the information about the ligand-protein contact became more clear and those interactions which were very unstable but somehow came in the docked pose were replaced by more stable interactions visible in the molecular dynamics results. Also, we infer some important regions in the proteins, where we observed fluctuations in the residues to some extent upon ligand binding.



SUPPLEMENTARY FIG. S3 (A); (B): LIGAND PROTEIN CONTACT 2D DIAGRAM FOR RITONAVIR (LEFT) AND LOPINAVIR (RIGHT)

CONCLUSION: Based on the computational study, we have selected three molecules that are diverse in nature. DB02307 belongs to the class of organic compounds known as dipeptides. These are organic compounds containing a sequence of exactly two alpha-amino acids joined by a peptide bond. DB04226 belongs to the class of organic compounds known as aminocyclitol glycosides. These are organic compounds containing an amicocyclitol moiety glycosidically linked to a carbohydrate moiety. DB01713 belongs to the class of organic compounds known as pyrimidine ribonucleoside diphosphates. Hence these diverse molecules can be taken as seed for designing potential main protease inhibitors. We even found out that most of the top scoring molecules belong to the dipeptide group, so designing either peptidomimetics or hybrid peptides can even be rational for inhibiting the main protease. An interesting analysis was observed that apart from the catalytic dyad there is a region in the main protease from residue 186 to 192 having an

important play in the binding of the ligand with the target. This inference, along with our selected three molecules, could be used as a basis for designing of main protease inhibitors using the repurposing approach.

ACKNOWLEDGEMENT: The authors thank the National Institute of Pharmaceutical Education and Research (NIPER), Department of Pharmacoinformatics, SAS Nagar, Ministry of Chemicals and Fertilizers, New Delhi, Government of India for providing the facility.

CONFLICTS OF INTEREST: The authors declare no potential conflict of interest.

REFERENCES:

1. Duan K, Liu B, Li C, Zhang H, Yu T, Qu J, Zhou M, Chen L, Meng S and Hu Y: Effectiveness of convalescent plasma therapy in severe COVID-19 patients. Proceedings of the National Academy of Sciences 2020; 117: 9490-96.
2. Talevi A: Drug repositioning: current approaches and their implications in the precision medicine era. Expert Review

- of Precision Medicine and Drug Development 2018; 3(1): 49-61.
3. Polamreddy P and Gattu N: The drug repurposing landscape from 2012 to 2017: evolution, challenges, and possible solutions. *Drug Discovery Today* 2019; 24(3): 789-95.
 4. Jourdan JP, Bureau R, Rochais C and Dallemagne P: Drug repositioning: a brief overview. *Journal of Pharmacy and Pharmacology* 2020; 72(9): 1145-51.
 5. Rosa S G V and Santos W C: Clinical trials on drug repositioning for COVID-19 treatment. *Revista Panamericana de Salud Pública* 2020; 44: e40.
 6. Oprea TI, Bauman JE, Bologna CG, Buranda T, Chigaev A, Edwards BS, Jarvik JW, Gresham, H D, Haynes M K and Hjelle B: Drug repurposing from an academic perspective. *Drug Discovery Today: Thera Strategies* 2011; 8: 61-69.
 7. Harrison C: Coronavirus puts drug repurposing on the fast track. *Nature biotechnology* 2020; 38: 379-81.
 8. Siddiqi H K and Mehra M R: COVID-19 illness in native and immunosuppressed states: A clinical–therapeutic staging proposal. *The Journal of Heart and Lung Transplantation* 2020; 39: 405.
 9. Sawicki SG, Sawicki DL and Siddell SG: A contemporary view of coronavirus transcription. *Journal of Virology* 2007; 81: 20-29.
 10. Ziebuhr J, Snijder EJ and Gorbalenya AE: Virus-encoded proteinases and proteolytic processing in the Nidovirales. *Journal of General Virology* 2000; 81: 853-79.
 11. Sheahan TP, Sims AC, Leist SR, Schäfer A, Won J, Brown AJ, Montgomery SA, Hogg A, Babusis D and Clarke MO: Comparative therapeutic efficacy of remdesivir and combination lopinavir, ritonavir, and interferon beta against MERS-CoV. *Nature communications* 2020; 11: 1-14.
 12. Kadam RU and Wilson IA: Structural basis of influenza virus fusion inhibition by the antiviral drug Arbidol. *Proceedings of the National Academy of Sciences* 2017; 114: 206-14.
 13. Liu C, Zhou, Q Li Y, Garner LV, Watkins SP, Carter L J, Smoot J, Gregg AC, Daniels AD and Jervey S: Research and development on therapeutic agents and vaccines for COVID-19 and related human coronavirus diseases. *ACS Publications* 2020: 315-31.
 14. Hoffmann M, Kleine-Weber H, Schroeder S, Krüger N, Herrler T, Erichsen S, Schiergens TS, Herrler G, Wu NH and Nitsche A: SARS-CoV-2 cell entry depends on ACE2 and TMPRSS2 and is blocked by a clinically proven protease inhibitor. *Cell* 2020; 181(2): 271-80.
 15. Arabi YM, Shalhoub S, Mandourah Y, Al-Hameed F, Al-Omari A, Al Qasim E, Jose J, Alraddadi B, Almotairi A and Al Khatib K: Ribavirin and interferon therapy for critically ill patients with middle east respiratory syndrome: a multicenter observational study. *Clinical Infectious Diseases* 2020; 70: 1837-44.
 16. Berman HM, Westbrook J, Feng Z, Gilliland G, Bhat TN, Weissig H, Shindyalov IN and Bourne PE: The protein data bank. *Nucleic Acids Research* 2000; 28: 235-42.
 17. Anand K, Palm GJ, Mesters JR, Siddell SG, Ziebuhr J and Hilgenfeld R: Structure of coronavirus main proteinase reveals combination of a chymotrypsin fold with an extra α -helical domain. *The EMBO journal* 2002; 21: 3213-24.
 18. Lim L, Shi J, Mu Y and Song J: Dynamically-driven enhancement of the catalytic machinery of the SARS 3C-like protease by the S284-T285-I286/A mutations on the extra domain. *PLoS One* 2014; 9: e101941.
 19. Zhang L, Lin D, Sun X, Curth U, Drosten C, Sauerhering L, Becker S, Rox K and Hilgenfeld R: Crystal structure of SARS-CoV-2 main protease provides a basis for design of improved α -ketoamide inhibitors. *Science* 2020; 368: 409-12.
 20. Douangamath A, Fearon D, Gehrtz P, Krojer T, Lukacik P, Owen CD, Resnick E, Strain-Damerell C, Aimon A, Ábrányi-Balogh P and Brandão-Neto J: Crystallographic and electrophilic fragment screening of the SARS-CoV-2 main protease. *Nature Communications* 2020; 11(1): 1-1.
 21. Schrödinger Release 2019-1: Glide, Schrödinger, LLC, New York, NY, 2020.
 22. Wishart DS, Feunang YD, Guo AC, Lo EJ, Marcu A, Grant JR, Sajed T, Johnson D, Li C, Sayeeda Z and Assempour N: DrugBank 5.0: a major update to the DrugBank database for 2018. *Nucleic Acids Res* 2018; 46: D1074-D1082.
 23. Schrödinger Release 2019-1: SiteMap, Schrödinger, LLC, New York, NY, 2019.
 24. Schrödinger Release 2019-1: Protein Preparation Wizard; Epik, Schrödinger, LLC, New York, NY, 2016; Impact, Schrödinger, LLC, New York, NY, 2016; Prime, Schrödinger, LLC, New York, NY, 2019.
 25. Schrödinger Release 2019-1: LigPrep, Schrödinger, LLC, New York, NY, 2019.
 26. Schrödinger Release 2019-1: Prime, Schrödinger, LLC, New York, NY, 2019.
 27. Pearlman DA: Evaluating the molecular mechanics Poisson-Boltzmann surface area free energy method using a congeneric series of ligands to p38 MAP kinase. *J Med Chem* 2005; 48: 7796-807.
 28. Schrödinger Release 2019-1: Desmond Molecular Dynamics System, D. E. Shaw Research, New York, NY, 2019. Maestro-Desmond Interoperability Tools, Schrödinger, New York, NY, 2020.

How to cite this article:

Sobhia ME, Ghosh K, Sivangula S and Kumar GS: Deciphering Covid-19 enigma by targeting Sars-Cov-2 main protease using *in-silico* approaches. *Int J Pharm Sci & Res* 2021; 12(6): 3104-19. doi: 10.13040/IJPSR.0975-8232.12(6).3104-19.

All © 2013 are reserved by the International Journal of Pharmaceutical Sciences and Research. This Journal licensed under a Creative Commons Attribution-NonCommercial-ShareAlike 3.0 Unported License.

This article can be downloaded to **Android OS** based mobile. Scan QR Code using Code/Bar Scanner from your mobile. (Scanners are available on Google Playstore)